AIP Advances

Nanopatterned metallic transparent electrodes for the near-infrared spectrum

Cite as: AIP Advances **11**, 045005 (2021); https://doi.org/10.1063/5.0044447
Submitted: 16 January 2021 . Accepted: 14 March 2021 . Published Online: 01 April 2021

Aliaksandr Hubarevich, Mikita Marus, Yauhen Mukha, Aliaksandr Smirnov, and Xiao Wei Sun

Nanopatterned metallic transparent electrodes for the near-infrared spectrum

Cite as: AIP Advances 11, 045005 (2021); doi: 10.1063/5.0044447
Submitted: 16 January 2021 • Accepted: 14 March 2021 •
Published Online: 1 April 2021

Aliaksandr Hubarevich,[1,a)] Mikita Marus,[1,2] Yauhen Mukha,[1] Aliaksandr Smirnov,[1] and Xiao Wei Sun[2,b)]

AFFILIATIONS

[1] Laboratory for Information Display and Processing Units, Belarusian State University of Informatics and Radioelectronics, 6 P. Brovki, 220013 Minsk, Belarus

[2] Guangdong Higher Education Key Lab of Advanced Quantum Dot Displays and Lighting, Shenzhen Key Laboratory of Advanced Quantum Dot Displays and Lighting, and Department of Electrical and Electronic Engineering, Southern University of Science and Technology (SUSTech), 1088 Xueyuan Avenue, 518055 Shenzhen, People's Republic of China

[a)] hubarevich@bsuir.by
[b)] **Author to whom correspondence should be addressed:** sunxw@sustech.edu.cn

ABSTRACT

Near-infrared transparent electrodes constitute an essential component of light-emitting and photovoltaic devices widely employed in short- and long-range communication, light detection and ranging, biodiagnostics, security, virtual and augmented reality, night vision, gas sensing, and solar cells. However, the efficiency of all these devices and related applications suffers from significantly reduced transmittance of the indium tin oxide electrode compared to the visible wavelength range. Here, we explore the potential of randomly and uniformly arranged silver, gold, and aluminum nanopore and nanowire films for the near-infrared optoelectronics. We show that these metallic nanopatterned layers, except for randomly arranged nanoporous configurations, exhibit considerably higher performance than the commonly used indium tin oxide. Furthermore, silver layers possess higher transmittance and lower haze than gold and aluminum ones, while the nanowire configuration overperforms the nanoporous one. The obtained results offer a means for deeper analysis of metallic nanopatterned transparent electrodes for many near-infrared optoelectronic applications.

I. INTRODUCTION

Near-infrared (NIR) transparent electrodes possess a crucial component of many current and future optoelectronic devices. The NIR spectrum accounts for more than half (52%) of the solar energy used in photovoltaics.[1] NIR quantum dot-based light-emitting diodes (NIR QLEDs) offer strong benefits for night vision, optical communications, and biomedical applications.[2,3] The optoelectronic performance of all those NIR devices heavily relies on the transparent electrode and is currently limited by the widely used indium tin oxide (ITO) electrode.[4] The transmittance of ITO significantly drops in the near-infrared (NIR) spectrum as the plasma frequency of ITO occurs in NIR, which makes ITO transparent in the visible spectrum but reflective in NIR.[5] Patterning of ITO improves the transmittance but also increases the sheet resistance and thus limits an application area.[6]

Metallic nano- and micropatterned layers have shown themselves as a promising candidate for the next-generation transparent electrode.[7–11] In addition to excellent optoelectrical properties in the visible spectrum, they benefit from flexibility,[12–14] stretchability,[15–17] and low fabrication cost.[18–20] Moreover, recent results indicate that silver nanowire (AgNW) layers possess high transmittance in NIR as well.[21]

Here, we studied randomly and uniformly arranged nanoporous and nanowire configurations of silver (Ag), gold (Au), and aluminum (Al) layers to deeply investigate their transmittance, haze, and sheet resistance in NIR and compare them to ITO. We found that Ag, Au, and Al nanopatterned layers exhibit significantly higher performance than ITO and are well suited as transparent electrodes for many NIR applications.

II. METHODOLOGY

A. Experiments

AgNWs were synthesized at 160 °C in an automated synthesis chamber using the polyol process.[22] Silver nitrate ($AgNO_3$), ethylene

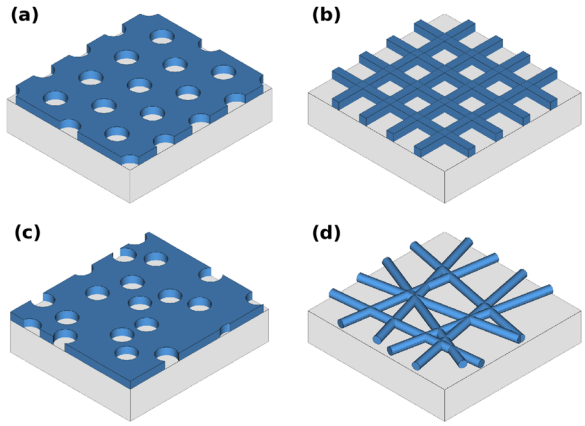

FIG. 1. Geometrical models of the uniformly [(a) and (b)] and randomly [(c) and (d)] arranged porous and wire metallic patterned layers on a substrate.

glycol (EG), copper chloride, and polyvinylpyrrolidone (PVP) were used as starting materials, and the synthesis processes are detailed elsewhere.[23] The as-synthesized AgNWs were cleaned three times in isopropanol (IPA) and then redispersed in deionized (DI) water. AgNW ink was formulated at 3 mg/ml Ag concentration in DI water. The AgNW ink was coated over a 150 mm-width polyethylene terephthalate (PET) flexible substrate on a Coatema roll-to-roll smart coater with a slot die at a coating speed of 0.2 m/min and was dried at 150 °C. AgNW loading density (LD) was controlled by adjusting the ink feeding rate to the slot-die coater. The as-coated films were cut into 5 × 5 cm^2 samples for characterization. The sheet resistance was measured using a Delcom Instruments benchtop contactless probe. Optical measurements were performed using the PerkinElmer Lambda 750S UV/Vis/NIR spectrophotometer for the wavelength range of 800–2400 nm.

B. Simulations

Figure 1 shows the geometrical models of the uniformly and randomly arranged porous and wire metallic nanopatterned layers on a substrate. PET was used as the substrate material, and silver, gold, and aluminum were used as the materials for metallic patterned layers. Optical constants of PET were taken from Refs. 24 and 25. The thickness of nanopatterned layers was set to 30, 60, and 90 nm as they are the most used diameters for silver nanowires, and their surface area was changed from minimum to maximum values, i.e., when conductivity changed from near zero to the bulk value.

A commercial-grade simulator based on the finite-difference-time-domain (FDTD) method was used to perform the optical calculations.[26] The refractive index and extinction coefficient of the metals were taken from Ref. 27, and the glass refractive index was set to 1.52. The incident light from 0.8 to 2.4 μm was illuminated along the z-axis. The periodic boundary conditions and perfectly matched layers were applied perpendicular and parallel to the z-axis, respectively. The simulation unit cell area in the case of the random arrangement was set to 10, 20, and 30 μm for 30, 60, and 90 nm thick nanopatterned layers, respectively, and it was set to $a \times a$ and $a \times \sqrt{3}a$ for the wire and porous uniformly arranged layers, respectively, where a is the interwire or interpore distance. The simulation details for the transmittance, haze, and sheet resistance of the configurations mentioned above are described in our previous work.[28–32]

III. RESULTS AND DISCUSSION

The NIR spectrum is of interest for many applications such as solar cells (around 50% of the solar radiation occurs in NIR),

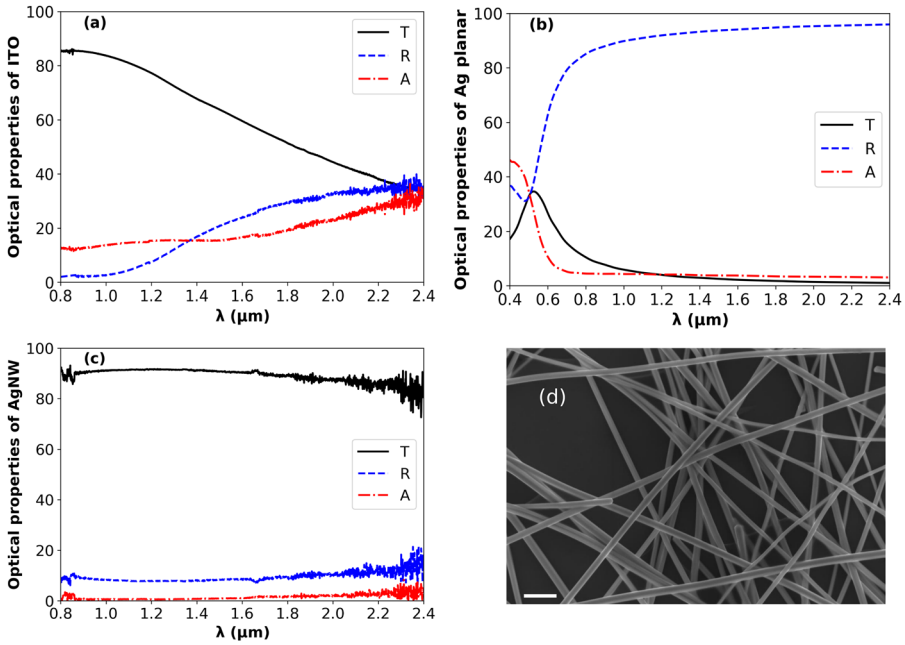

FIG. 2. Transmittance of ITO (a), Ag planar (b), and AgNW (c). (d) SEM image of AgNW (scale bar is 250 nm). The thickness and sheet resistance are 200 nm and 20 Ω/□ for ITO, 60 nm and 0.26 Ω/□ for Ag planar, and 60 nm and 20 Ω/□ for AgNW.

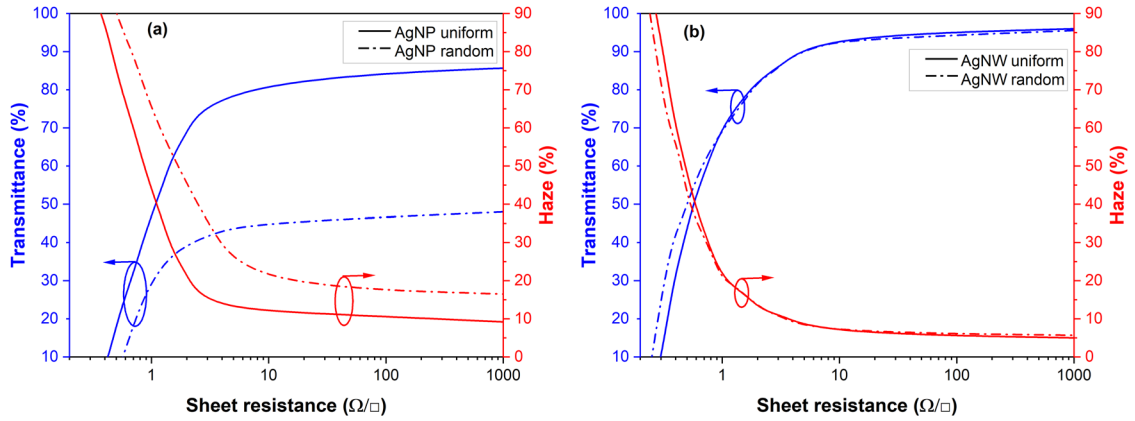

FIG. 3. Average transmittance and haze against the sheet resistance for the 60 nm thick uniformly and randomly arranged AgNP (a) and AgNW (b) layers.

night vision, optical communications, and biological and medical sensors.[2,3,33,34] The plasma frequency of ITO can be tuned through different tin (Sn) doping concentrations in tin oxide (SnO_2), which is an electron donor. The maximum carrier concentration around 10^{21} can be achieved;[35] further doping increases the sheet resistance due to disorders in the indium oxide (In_2O_3) lattice, which enhances phonon and ionized impurity scattering.[36] The plasma frequency of ITO occurs in NIR, making the transmittance above 80% in the visible spectrum. Simultaneously, it significantly drops in NIR due to increased reflectance and absorbance, as shown in Fig. 2(a). A similar effect demonstrates the Ag planar layer in the visible spectrum, as the plasma frequency of Ag occurs in the ultraviolet range [Fig. 2(b)]. It is important to note that Ag, Au, and Al planar layers have around 10^4 lower sheet resistance than ITO, and thus, they can be nanopatterned to outperform ITO. Figures 2(c) and 2(d) show NIR transmittance and SEM image of the 60 nm thick Ag nanowire layer (AgNW). AgNW transmits around 90% over the whole spectrum, while ITO transmittance drops from 85% to 35%, although the sheet resistance is 20 Ω/□ for both layers.

To investigate different configurations of the patterned layers, we simulated the average transmittance and haze against the sheet resistance for the 60 nm thick uniformly and randomly arranged Ag nanoporous (AgNP) and AgNW layers, as shown in Fig. 3. The random AgNP exhibits 45% transmittance at 10 Ω/□, which is less than

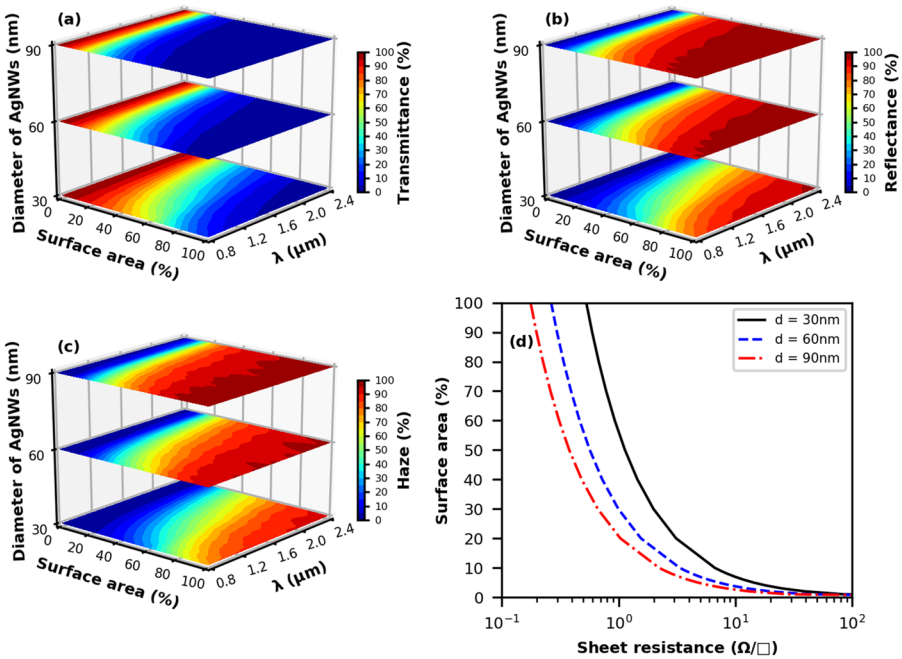

FIG. 4. The simulated transmittance (a), reflectance (b), haze (c), and sheet resistance (d) for the 30, 60, and 90 nm thick AgNW electrodes.

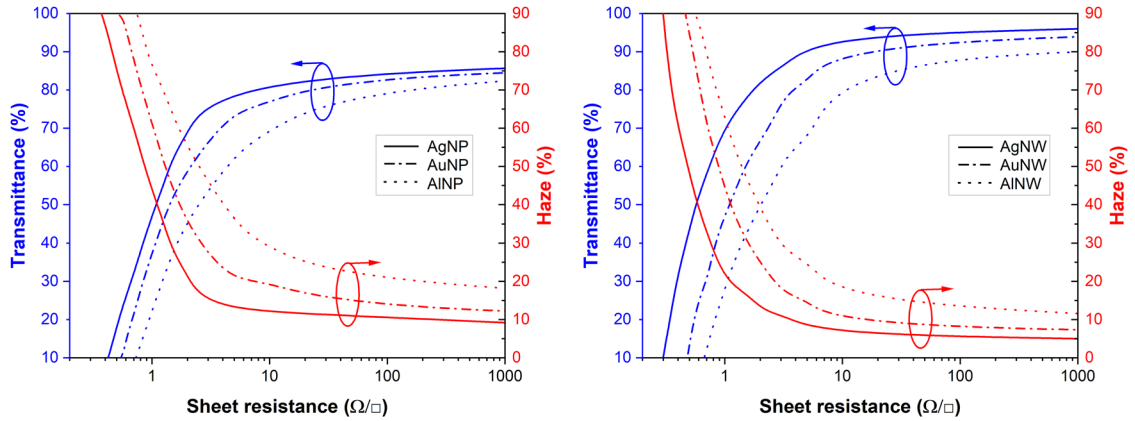

FIG. 5. Transmittance and haze for Ag, Au, and Al uniformly arranged nanopatterned layers. The thickness for all layers is 60 nm.

ITO. Such a low-performance results from the minimum surface area (i.e., when the conductivity is zero) of around 40% for randomly arranged porous layers,[37,38] limiting the transmittance. The uniform AgNP with the hexagonal arrangement covers 9% minimum surface area and hence reaches higher transmittance—80% at 10 Ω/□. Owing to the same reason, random AgNP exhibits 20% haze at 10 Ω/□, while the uniform one has 10%. Both uniform and random AgNW reach 90% transmittance and 7% haze at 10 Ω/□, thereby outperforming the AgNP configuration as the minimum surface area for AgNW approaches zero.

Figure 4 shows the simulated optoelectronic performance for 30, 60, and 90 nm thick AgNW electrodes. The surface area between 5% and 10% is needed to obtain the transmittance above 80% and haze below 10% at 10 Ω/□, which suits many applications. The surface area above 10% significantly decreases the transmittance due to the increased reflectance and haze. The thickening of AgNW requires a reduction of the surface area to keep the aforementioned performance. For instance, increasing the thickness of AgNW from 30 to 90 nm requires reducing the surface area from 10% to 5% and increasing the interwire distance from 585 to 1705 nm. Further thickening of AgNW commands even a larger interwire distance and thus limits the application area.

Figure 5 compares the simulated average transmittance and haze for 60 nm thick Ag, Au, and Al nanopatterned layers with the uniform arrangement. Both AuNP and AuNW possess a similar transmittance to Ag ones, but slightly lower conductivity, and as a result, their transmittance and haze are 77% and 12% for the porous configuration and 87% and 10% for the wire configuration at 10 Ω/□. AlNP and AlNW possess both lower transmittance and conductivity than Ag ones, and as a result, their transmittance and haze are 70% and 25% for the porous configuration and 80% and 20% for the wire configuration at 10 Ω/□. In summary, Ag, Au, and Al nanopatterned layers (with the exception of randomly arranged nanoporous ones) exhibit significantly higher performance than ITO and are well suited as transparent electrodes for many NIR applications.

IV. CONCLUSION

We investigated the randomly and uniformly arranged nanoporous and nanowire configurations of Ag, Au, and Al layers as NIR transparent electrodes. All those aforementioned metallic nanopatterned layers, except randomly arranged nanoporous ones, exhibit considerably higher optoelectronic performance than the commonly used ITO. The optical difference between the nanoporous and nanowire configurations depends on the minimum surface area, i.e., when conductivity approaches zero. Moreover, the surface area between 5% and 10% is needed to obtain the transmittance above 80% and haze below 10% at 10 Ω/□, which suits many NIR applications.

ACKNOWLEDGMENTS

A.H. and A.S. acknowledge funding from A. Kladov, Director of BAS Innovation Ltd. (Minsk, Belarus), the Belarusian Republican Foundation for Fundamental Research (Grant Nos. F19KITG-009 and T19PM-039), and State Programs of Scientific Research of the Republic of Belarus "Physical Materials Science, New Materials and Technologies" (2.45). X.W.S. received funding from the National Key Research and Development Program of China administrated by the Ministry of Science and Technology of China (Grant No. 2016YFB0401702), the Key-Area Research and Development Program of Guangdong Province (Grant No. 2019B010925001), the Shenzhen Key Laboratory for Advanced Quantum Dot Displays and Lighting (Grant No. ZDSYS201707281632549), and the Shenzhen Peacock Team Project (Grant No. KQTD2016030111203005).

DATA AVAILABILITY

The data that support the findings of this study are available from the corresponding author upon reasonable request.

REFERENCES

[1] L. Liu, A. Han, M. Ye, and W. Feng, Solar Energy **113**, 48 (2015).
[2] L. Sun, J. J. Choi, D. Stachnik, A. C. Bartnik, B.-R. Hyun, G. G. Malliaras, T. Hanrath, and F. W. Wise, Nat. Nanotechnol. **7**, 369 (2012).
[3] L. Gao, L. N. Quan, F. P. García de Arquer, Y. Zhao, R. Munir, A. Proppe, R. Quintero-Bermudez, C. Zou, Z. Yang, M. I. Saidaminov, O. Voznyy, S. Kinge, Z. Lu, S. O. Kelley, A. Amassian, J. Tang, and E. H. Sargent, Nat. Photonics **14**, 227 (2020).

[4]K. Ghaffarzadeh and R. Das, *Transparent Conductive Films and Materials 2019-2029: Forecasts, Technologies, Players* (IDTechEx Research, 2019).
[5]S. H. Brewer and S. Franzen, J. Phys. Chem. B **106**, 12986 (2002).
[6]K. Sakamoto, H. Kuwae, N. Kobayashi, A. Nobori, S. Shoji, and J. Mizuno, Sci. Rep. **8**, 2825 (2018).
[7]P. B. Catrysse and S. Fan, Nano Lett. **10**, 2944 (2010).
[8]D. S. Hecht, L. Hu, and G. Irvin, Adv. Mater. **23**, 1482 (2011).
[9]T. Sannicolo, M. Lagrange, A. Cabos, C. Celle, J.-P. Simonato, and D. Bellet, Small **12**, 6052 (2016).
[10]B. Han, K. Pei, Y. Huang, X. Zhang, Q. Rong, Q. Lin, Y. Guo, T. Sun, C. Guo, D. Carnahan, M. Giersig, Y. Wang, J. Gao, Z. Ren, and K. Kempa, Adv. Mater. **26**, 873 (2014).
[11]L. Hu, H. Wu, and Y. Cui, MRS Bull. **36**, 760 (2011).
[12]M. S. Miller, J. C. O'Kane, A. Niec, R. S. Carmichael, and T. B. Carmichael, ACS Appl. Mater. Interfaces **5**, 10165 (2013).
[13]L. Zhou, H.-Y. Xiang, S. Shen, Y.-Q. Li, J.-D. Chen, H.-J. Xie, I. A. Goldthorpe, L.-S. Chen, S.-T. Lee, and J.-X. Tang, ACS Nano **8**, 12796 (2014).
[14]S. Nam, M. Song, D.-H. Kim, B. Cho, H. M. Lee, J.-D. Kwon, S.-G. Park, K.-S. Nam, Y. Jeong, S.-H. Kwon, Y. C. Park, S.-H. Jin, J.-W. Kang, S. Jo, and C. S. Kim, Sci. Rep. **4**, 4788 (2014).
[15]B. W. An, E.-J. Gwak, K. Kim, Y.-C. Kim, J. Jang, J.-Y. Kim, and J.-U. Park, Nano Lett. **16**, 471 (2016).
[16]P. Lee, J. Lee, H. Lee, J. Yeo, S. Hong, K. H. Nam, D. Lee, S. S. Lee, and S. H. Ko, Adv. Mater. **24**, 3326 (2012).
[17]C. Zhang, A. Khan, J. Cai, C. Liang, Y. Liu, J. Deng, S. Huang, G. Li, and W.-D. Li, ACS Appl. Mater. Interfaces **10**, 21009 (2018).
[18]J.-Y. Lee, S. T. Connor, Y. Cui, and P. Peumans, Nano Lett. **8**, 689 (2008).
[19]J. Schneider, P. Rohner, D. Thureja, M. Schmid, P. Galliker, and D. Poulikakos, Adv. Funct. Mater. **26**, 833 (2016).
[20]S. Lin, X. Bai, H. Wang, H. Wang, J. Song, K. Huang, C. Wang, N. Wang, B. Li, M. Lei, and H. Wu, Adv. Mater. **29**, 1703238 (2017).
[21]J. Atkinson and I. A. Goldthorpe, Nanotechnology **31**, 365201 (2020).
[22]Y. Sun and Y. Xia, Adv. Mater. **14**, 833 (2002).
[23]F. N. Kholid, H. Huang, Y. Zhang, and H. J. Fan, Nanotechnology **27**, 025703 (2015).
[24]X. Zhang, J. Qiu, X. Li, J. Zhao, and L. Liu, Appl. Opt. **59**, 2337 (2020).
[25]X. Zhang, J. Qiu, J. Zhao, X. Li, and L. Liu, J. Quant. Spectrosc. Radiat. Transfer **252**, 107063 (2020).
[26]Lumerical Solutions, Inc., Canada, https://www.lumerical.com/products/fdtd/.
[27]A. D. Rakić, A. B. Djurišić, J. M. Elazar, and M. L. Majewski, Appl. Opt. **37**, 5271 (1998).
[28]M. Marus, A. Hubarevich, H. Wang, A. Smirnov, X. Sun, and W. Fan, Opt. Express **23**, 6209 (2015).
[29]M. Marus, A. Hubarevich, H. Wang, A. Stsiapanau, A. Smirnov, X. W. Sun, and W. Fan, Opt. Express **23**, 26794 (2015).
[30]A. Hubarevich, M. Marus, W. Fan, A. Smirnov, X. W. Sun, and H. Wang, Opt. Express **23**, 17860 (2015).
[31]A. Hubarevich, M. Marus, Y. Mukha, K. Wang, A. Smirnov, and X. W. Sun, AIP Adv. **9**, 045226 (2019).
[32]M. Marus, A. Hubarevich, H. Wang, Y. Mukha, A. Smirnov, H. Huang, W. Fan, and X. W. Sun, Thin Solid Films **626**, 140 (2017).
[33]E. H. Sargent, Adv. Mater. **20**, 3958 (2008).
[34]Z. C. Holman, M. Filipič, A. Descoeudres, S. De Wolf, F. Smole, M. Topič, and C. Ballif, J. Appl. Phys. **113**, 013107 (2013).
[35]H. Kim, C. M. Gilmore, A. Piqué, J. S. Horwitz, H. Mattoussi, H. Murata, Z. H. Kafafi, and D. B. Chrisey, J. Appl. Phys. **86**, 6451 (1999).
[36]M. Mizuhashi, Thin Solid Films **70**, 91 (1980).
[37]B. J. Last and D. J. Thouless, Phys. Rev. Lett. **27**, 1719 (1971).
[38]M. F. Sykes and J. W. Essam, Phys. Rev. **133**, A310 (1964).